Single Neurons can Induce Phase Transitions of Cortical Recurrent Networks with Multiple Internal States

Shigeyoshi Fujisawa, Norio Matsuki, and Yuji Ikegaya*

Laboratory of Chemical Pharmacology, Graduate School of Pharmaceutical Sciences,
The University of Tokyo, Tokyo 113-0033, Japan

Abbreviated title: Phase Transitions of Cortical Recurrent Networks

Manuscript includes 40 pages of typescript and 9 figures
(240 words in the abstract, 463 words in the introduction, 1544 words in the discussion)

* Correspondence should be addressed to Yuji Ikegaya.
Laboratory of Chemical Pharmacology, Graduate School of Pharmaceutical Sciences,
The University of Tokyo, 7-3-1 Hongo, Bunkyo-ku, Tokyo 113-0033, Japan.
E-mail: ikegaya@tk.air.jp, Phone & Fax: +81-3-5841-4783

KEY WORDS
Phase transition; UP state; Self-organization; Hippocampus; Microcircuit; Recurrent Network

Acknowledgements
The authors are grateful to Prof. Rafael Yuste (Columbia University) and Mr. Brendon O. Watson (Columbia University) for their critical review on an early version of the manuscript, and to Prof. Takuya Sakaguchi (Kurashiki University of Science and the Arts) for his technical comments on streptavidin labeling. This work was supported in part by Grant-in-Aid for Science Research from the Ministry of Education, Culture, Sports, Science and Technology of Japan.

ABSTRACT

Fluctuations of membrane potential of cortical neurons, referred here to as internal states, are essential for brain function, but little is known about how these internal states emerge and are maintained or what determines transitions between these states. We performed intracellular recordings from hippocampal CA3 pyramidal cells *ex vivo* and found that neurons display multiple and hierarchical internal states, which are linked to cholinergic activity and are characterized by several power law structures in membrane potential dynamics. Multiple recordings from adjacent neurons revealed that the internal states were coherent between neurons, indicating that the internal state of any given cell in a local network could represent the network activity state. Repeated stimulation of single neurons led over time to transitions to different internal states in both the stimulated neuron and neighboring neurons. Thus, single cell activation is sufficient to shift the state of the entire local network. As the states shift to more active levels, theta- and gamma-frequency components developed in the form of subthreshold oscillations. State transitions were associated with changes in membrane conductance but were not accompanied by a change in reversal potential. These data suggest that the recurrent network organizes the internal states of individual neurons into synchronization through network activity with balanced excitation and inhibition and that this organization is dynamic and has multiple levels. Thus, neuronal states reflect the "phase" of an active network, a novel demonstration of the dynamics and flexibility of cortical microcircuitry.

INTRODUCTION

Cognitive functions of humans and animals, including consciousness, perception, learning, and memory retrieval, depend on brain states (Wilson and McNughton 1994; Vaadia et al., 1995; Steriade et al., 2001; Stickgold et al., 2001). Such brain states emerge spontaneously during behavior as well as the wake-sleep cycle, and they are ultimately attributed to fluctuations of membrane potential of individual neurons (both suprathreshold and subthreshold). These fluctuations are referred to here as internal states. One of the representative internal states is slow-wave oscillations, so-called UP/DOWN alternations. The UP/DOWN alternations are characterized by a low-frequency (< 1 Hz) and large-amplitude (~20 mV) alternation of depolarization and hyperpolarization, and they are usually observed in slow-wave sleep and under anesthesia (Steriade et al., 1993; Cowan and Wilson, 1994). These states influence neural processing of sensory inputs, that is, the intensity and propagation of neuronal activity vary depending on whether neurons reside in UP or DOWN (Anderson et al., 2000; Petersen et al., 2003; Shu et al., 2003b; Sachdev et al., 2004; Brecht et al., 2004; Leger et al., 2005). In the waking state or rapid-eye-movement (REM) sleep, the UP/DOWN alternation disappears, and instead, neurons display persistent UP depolarization with fast oscillations (Steriade et al., 2001; Steriade 2003). In the hippocampus, this state is likely to be associated with theta-frequency (3-7 Hz) oscillations (Buzsaki, 2002).

Thus, neurons possess various internal states, but it remains to be elucidated how neurons generate, maintain and transit between these internal states. Previous studies have demonstrated that ongoing fluctuations of membrane potential are synchronized among adjacent neurons in the hippocampus (Kamondi et al., 1998; Buzsaki 2002), the neocortex (Lampl et al., 1999; Petersen et al., 2003; Ikegaya et al., 2004), and the striatum (Stern et al., 1998). Network synchrony is believed to depend on recurrent synaptic activity with a balance of excitation and inhibition (Amit and Brunel, 1997; Shu et al., 2003a). In the present study, therefore, we first focus on the

relationship of synchronous synaptic inputs and the internal states of hippocampal CA3 pyramidal cells, which synapse with approximately 6,000 other pyramidal cells to form an autoassociative, recurrent network *in vivo* (Amaral et al., 1990). We then closely examine the temporal structures and dynamics of the internal states observed in these neurons. We find that membrane potential dynamics of nearby neurons are coherent, have many degrees of intensity, and are organized with multiple power law structures. We create a theoretical model that is analogous to the Landau "phase transition" theory and replicates the dynamics of the internal states of a neuron. The computer simulation suggests that the level of balanced excitatory and inhibitory inputs is crucial for determining the internal states. We therefore propose that the internal states of neurons represent the "phase" of an active recurrent network, i.e., a synchronous network state.

MATERIALS AND METHODS

Organotypic cultures of hippocampal slices

Hippocampal slices prepared from postnatal day 7 Wistar/ST rats (SLC, Shizuoka, Japan) were cultured as previously described (Koyama et al., 2004). Briefly, rat pups were deeply anesthetized by hypothermia, and their brains were aseptically removed, according to the National Institutes of Health guidelines for laboratory animal care and safety. The caudal half of the whole brain was horizontally cut into 300-μm-thick slices using a DTK-1500 vibratome (Dosaka, Kyoto, Japan) in aerated, ice-cold Gey's balanced salt solution supplemented with 25 mM glucose. The entorhino-hippocampi were dissected out under stereomicroscopic controls and cultivated using the membrane interface technique. Slices were placed on sterile 30-mm-diameter membranes (Millicell-CM, Millipore, Bedford, MA). Cultures were fed with 1 ml of 50% minimal essential medium (Invitrogen, Gaithersburg, MD), 25% horse serum (Cell Culture Lab, Cleveland, OH) and 25% Hanks' balanced salt solution and maintained in a humidified incubator at 37°C in 5% CO_2. The medium was changed every 3.5 days. Electrophysiological experiments were performed at

day 9-14 in vitro.

Electrophysiological recordings

Whole-cell recording was performed as described elsewhere (Fujisawa et al. 2004a). A slice was transferred to a recording chamber and continuously perfused with oxygenated artificial CSF consisting of (mM): 124 NaCl, 25 $NaHCO_3$, 3 KCl, 1.24 KH_2PO_4, 1.4 $MgSO_4$, 2.2 $CaCl_2$, and 10 glucose (37°C). Micropipettes (4-7 MΩ) were filled with internal solutions consisting of (in mM): 136.5 $KMeSO_4$, 17.5 KCl, 9 NaCl, 1 $MgCl_2$, 10 HEPES, and 0.2 EGTA (pH 7.2). Tight-seal whole-cell recordings were obtained from CA3 pyramidal neurons under a differential interference contrast microscopy. Recordings were carried out with an Axopatch 200B amplifier (Axon Instruments, Foster City, CA). Signals were low-pass filtered at 1 kHz, digitized at 10 kHz and analyzed with pCLAMP 8.0 software (Axon Instruments). The sorting of post-synaptic potentials (PSPs) was carried out with custom-made software in Igor.

We report the mean ± standard deviation (SD) in all measurements.

Phase transition models

The details are shown in the supplemental material.

RESULTS

Transitions of active patterns of CA3 pyramidal cells

Hippocampal CA3 pyramidal cells make synapses with other CA3 pyramidal cells, forming an autoassociative, recurrent network in this area (Amaral et al., 1990). In cultured hippocampal slices, we found that out of 42 whole-cell recordings from pairs of visually identified CA3 pyramidal cells located within 300 μm, 23.8% (10/42) showed monosynaptic connection. This probability is compatible with the density of CA3 recurrent network in vivo (Gomez-Di Cesare et al., 1997).

A CA3 pyramidal neuron in cultured hippocampal slices was held in a current clamp mode of

whole-cell recordings. In order to activate this cell synaptically, we stimulated the stratum radiatum, where CA3 pyramidal cells project the associational fibers and provide recurrent inputs (Amaral et al., 1990). During 2 sec of 10-Hz stimulation, the recorded neurons generated burst spikes, and these burst discharges disappeared when the stimulation was terminated (n=5 slices, Fig. 1A control). We repeated the same paradigm of experiments in the presence of carbachol, a muscarinic receptor agonist, which is known to induce oscillatory activity in hippocampal slices (Fisahn et al., 1998; Traub et al., 2004; Fujisawa et al., 2004a). When the stratum radiatum was stimulated at 10 Hz for 2 sec in the presence of 10 μM carbachol, the membrane potentials of CA3 cells shifted to more positive potentials by 8.7 to 15.6 mV, and this depolarization was maintained and accompanied by persistent firing activity (n = 5 slices, Fig. 1A carbachol). On average, these self-sustained discharges lasted for 37.8 ± 19.7 sec (SD) and were spontaneously settled into the resting conditions. Similar persistent activities were obtained by current injection into recorded cells. In figure 1B, we injected a 5 second duration current that mimicked the temporal features of a barrage of post-synaptic potentials (PSPs) and found that this stimulus alone was sufficient to induce self-sustained tonic discharges (n=7 slices). This persistent activity was not induced in the absence of carbachol (n=5 slices). All subsequent experiments were performed in the presence of 10 μM carbachol (Fig. 1B).

In order to reveal any intermediate states between the resting state and the tonic discharge state, we applied a sequence of brief stimulation pulses (500 msec, rectangular 400 pA, every 10 sec), a protocol inspired by an analogous method used by Egorov et al. (2002). In 66 of 71 slices, the repetitive stimuli led to graded transitions of spontaneous firing patterns (Fig. 1C). In most cases, the amplitude of spikes was reduced after the induction of persistent activity (Fig. 1), but this was not due to a damage or degeneration of neurons because the spike size was reversed to the control level when the persistent activity was terminated by hyperpolarizing current injection (supplemental Fig. 1). The graded transitions of firing pattern were completely blocked by 1 μM

atropine, a cholinergic muscarinic receptor antagonist (n=5 slices; Fig. 1C) or by removal of extracellular Ca^{2+} (n=6 slices; data not shown).

Internal states *in vivo*, such as slow wave oscillations, are often characterized by an alternation of resting (DOWN) and depolarized (UP) membrane potentials (Steriade et al., 1993; Cowan and Wilson, 1994), and persistent firing activity may be explained by prolonged versions of UP depolarization (Steriade et al., 2001). We therefore considered that the duration of depolarizing shifts may serve as a dimension along which to evaluate the internal states. During the course of a repetitive stimulation experiment, membrane voltages yielded a bimodal distribution that was approximated by two Gaussian curves, using least squares fitting (Fig. 2A right); the first peak (blue line) corresponded to the resting membrane potential, and the second peak (red line) to the depolarized UP potential (Fig 2A). We defined a "significant depolarizing shift (SDS)" as any depolarization above the 0.1% significance level of the Gaussian distribution representing the resting potential (blue broken line). For example, the period indicated in red on the intracellular trace in the left panel of figure 3A represents an SDS. Note that SDSs were not confined only to UP depolarizations but include spikes and large PSPs. During SDSs, firing rates were initially high (> 10 Hz) and rapidly reduced to a plateau level at 4-5 Hz (theta rhythm) (Fig. 2B).

Figure 2C indicates a typical change in SDS durations following repetitive stimuli. A sequence of current injections gradually recruited this neuron into longer SDSs, eventually leading to a persistent SDS (Fig. 2C). Data for four other cells are summarized in figure 2D, where each color indicates each neuron.

Multiple internal states emerge in a self-organized manner.

Although the internal states could emerge as a continuum from the static state to persistent activity (but see below), we tried to expediently classify these internal states in order to analyze their structures and dynamics. We sought to categorize internal states based on the dynamics of

SDSs; a demonstration of this is shown in figure 3A. First we arbitrarily segmented an intracellular trace into consecutive time epochs of 10 sec and measured the lengths of all SDSs that occurred during each epoch (Fig. 3A left). We then selected the SDS with the maximal length in each 10-sec section, and we used that to classify the epoch into one of five states as follows. An epoch was defined as being in state I if the maximal SDS was less than 100 msec and no spike occurred during the 10-sec period. An epoch was defined as being in state II if the maximal SDS was less than 100 msec and at least one spike occurred. Epochs were defined as being in states III, IV and V if the maximal SDS was between 100 msec and 1 sec, between 1 sec and 10 sec, and 10 sec, respectively (Fig. 3A right). In the left panel of figure 3B, we show an example of membrane potential for each state. The histogram of membrane potential (Fig. 3B left, the inset) indicates that states I/II and state V correspond to persistent DOWN and persistent UP states, respectively, and that state IV shows clear bimodal UP/DOWN and represents an intermediate state.

To investigate the inner structures of these states, we created a histogram of the length of SDSs (Fig. 3Ba). Neuronal states were elicited by repeated stimulation pulses (see Fig. 2C,D), and data were collected from 34 cells. Power law structures were found in states from I to IV; the best fit was seen in state IV with an exponent (ν) of 1.43. Interestingly, however, SDS durations seen in individual neurons usually showed a multi-peaked distribution, the peak points in which varied from cell to cell (Fig. 2E). This suggests that the dynamics of membrane fluctuation is multistable and diverse at the single cell level.

We then examined the temporal patterns of spontaneous spikes. Figure 3Bb indicates the histograms of inter-spike intervals (ISIs). The ISI histogram of state II showed two peaks; the first peak at hundreds of milliseconds corresponded roughly to within-burst spike intervals, and the second peak in the orders of seconds corresponded to inter-burst intervals. The first peak grew in state III, and a $1/s^{\nu}$ structure emerged in state IV ($\nu = 1.33$). In state V, ISIs converged into the

220-msec peak, which corresponds to the theta rhythm.

To determine more about the temporal structure of a series of spikes, we created a first-return map of ISIs, in which individual ISIs were plotted versus the next ISIs (Fig. 3Bc). In general, if ISIs are random or irregular, their data points are uniformly scattered in the space of a return map, whereas if the spiking is regular the data cluster into one or a few point(s). On the other hand, when the data are aligned but in a non-linear pattern, the spiking pattern may be governed by certain non-linear, but deterministic, process (Ott, 1993; Fujisawa et al., 2004b).

The return map of ISIs in state II converged on the diagonal line of the ISI_i and ISI_{i+1} axes, and the state III map showed four convergence points, suggesting that neurons in these states fired spikes in a relatively regular manner. In state IV, however, the map showed a nonlinear function; ISI points were distributed in an inverse-U form peaking at about 500 ms, which suggest the existence of a non-linear process that controls spike sequences. Similar nonlinear behaviors of spikes were reported in the hippocampus in exploring rats *in vivo* (Harris et al., 2001). In state V, ISIs converged around the 220-ms interval. Taken together, different states had different inner structures leading to different spiking signatures.

We quantified the probability of state transitions between neighboring 10-sec segments of intracellular traces (n=34 slices). Figure 4A illustrates our method to estimate the transition probability; in the case of 'without stimulation', we arbitrarily segmented an intracellular trace into consecutive time epochs of 10 sec and classified each epoch into one of five states as defined above (see Fig. 3A). We then collected data and calculated the rate of state transitions that occurred between the 10-sec epochs (Fig. 4A top). In the case of 'with stimulation', we performed current injection every 10 sec, and compared the states before and after the stimulus (Fig. 4A bottom).

Figure 4B summarizes the probability that the state transition occurred spontaneously without stimulation (left) or were evoked by stimulation pulses (right). In both cases, neurons

tended to maintain their internal states that were the same as ones in the previous 10-sec period. Thus, the states per se are stable, which is suggestive of the presence of local attractors. As compared with unstimulated neurons, however, the rates of state transitions were significantly higher in neurons that received stimulation pulses, in which cases the states tended to transit to higher stages ($P<0.01$; Kolmogorov-Smirnov test).

Taken together, these data show that neurons possess multiple internal states between which they can dynamically drift. We differentiated these internal states by compiling and comparing the durations of all observed SDSs. Neurons at different states displayed different dynamics of subthreshold and suprathreshold membrane potential. Therefore, the neuronal states were plausibly classified by our definition, although the definition might seem to be arbitrary. In particular, state IV represents a unique, intermediate stage, which was characterized by several complex behaviors, including some power law structures and U-shaped ISI correlations.

Network states control the gain and responsiveness of neurons

To address whether network states influence information processing, we examined the response of a neuron with different states to stimulation of the mossy fibers, one of the major external inputs to the CA3 recurrent network. We applied trains of 10 field stimuli (80 μA, 50 msec) to the granule cell layer at various frequencies ranging from 0.4 to 100 Hz while the recorded neurons stayed in state I to IV. Representative intracellular traces are shown in figure 5A, and data for 7 slices were summarized in figure 5B, in which the ordinate indicates an output/input gain, defined by dividing the number of spike outputs by the number of input stimuli (i.e., 10). We did not analyze the state V because it was difficult to discriminate evoked spikes from spontaneous firing; note that this analysis was simply based on the question how many spikes are evoked by one stimulus (“gain”), so persistent spike activity during state V made this analysis impossible.

In state I, neurons fired very few spikes in response to low- and high-frequency stimulation

of the mossy fibers, whereas they responded more faithfully to individual stimuli in the middle ranges of frequency (4-10 Hz). As a result, state I neurons worked as a sort of band-pass filter (Fig. 5B left). In states II and III, neurons were more responsive to low frequency inputs (< 4 Hz) and acted like a low-pass filter (Fig. 5B left). For state IV, we analyzed UP and DOWN periods separately (Fig 5B right). When mossy fiber stimulation started during DOWN periods, the CA3 neurons responded very sensitively; the numbers of input stimuli and output spikes were almost equivalent at > 4 Hz of frequency (gain ≈ 1), and at lower frequencies, the neurons emitted multiple spikes than given inputs (gain > 1). On the other hand, when stimulation started during UP periods, the gain was less than 1 at high frequencies (> 10 Hz). Mossy fiber simulation usually terminated UP depolarization (Fig. 5A, and see also Shu et al., 2003a for the neocortex), and therefore, similar data were obtained for UP and DOWN at low frequencies (Fig. 5B right). These results indicate that different internal states have different modes of information processing.

In order to reveal the difference in responsiveness between UP and DOWN periods in state IV, we next measured the firing probability and the amplitude of EPSPs. The probability of firing in response of a single mossy fiber stimulus in DOWN was higher than in UP in state IV or state V (Supplemental Fig. 2A). We next examined the amplitude of mossy fiber-evoked EPSPs in DOWN and UP. The EPSP amplitude in DOWN was larger than that in UP (Supplemental Fig. 2B). Thus, the neuronal responsiveness was higher in DOWN than in UP periods, and this is in good agreement with previous studies in the neocortex *in vivo* (Petersen et al., 2003; Sachdev et al., 2004; Crochet et al., 2005; Leger et al., 2005; but see, Shu et al., 2003b).

State transitions are network-driven and can be triggered by activation of single cells

We addressed the cellular and network mechanisms of state transitions of CA3 pyramidal cells. Neuronal state shifts could not be induced in the presence of 20 μM CNQX, 50 μM D,L-AP5 and 100 μM PTX (Fig. 6A). Therefore, state transitions (or maintenance) require fast synaptic transmission and are unlikely to attribute to single cell attractors.

We performed paired recordings from neighboring CA3 pyramidal cells and applied repetitive stimulation pulses to one cell (cell1) alone. Strikingly, the stimulation induced state transitions in the other cell (cell2) as well as cell1 (Fig. 6B). The occurrence of SDSs was synchronized in time (figure 6B bottom left), and membrane potential fluctuations were also tightly correlated between two cells (figure 6B bottom right). Data for three other cells are shown in supplemental figure 3, and similar results were obtained in all cases tested. Data of all cell pairs recorded were summarized in figure 6C. In this figure, we calculated the overlap ratio of SDSs, which was defined as (the total duration of SDSs that occurred concurrently in cell1 and cell2)/$\sqrt{}${(the total SDS duration in cell1) × (the total SDS duration in cell2)}. Thus, the overlap ratio is 100% if SDSs are perfectly coincident between cell1 and cell2, whereas this value drops to 0% if SDSs are not synchronized at all. We plotted the overlap ratios as a function of the distance between two cells. Green and black dots indicate synaptically connected and unconnected cell pairs, respectively. SDSs became more synchronized as the states advanced to higher levels, and this synchronization was independent of the spatial distance between two cells recorded or of whether they had monosynaptic connections. Simultaneous intracellular and extracellular recordings also revealed that current injections into a single cell entrained the spiking dynamics of neuron populations in the surrounding network (supplemental figure 4).

Network activity is often associated with synchronized oscillations of membrane potential, such as theta (3~7 Hz) and gamma waves (30~80 Hz) (Buzsaki 2002; Traub et al., 2004). We explored how internal states are linked to subthreshold membrane potential oscillations, especially theta and gamma frequency components. Figure 7A shows membrane potential traces of cell1 (current-injected cell) and cell2 (unstimulated). The cross-correlogram of their subthreshold membrane potentials is shown below the traces, indicating that the correlation patterns varied between states. Fourier power spectra of this cross-correlogram (Fig. 7B) showed that theta-frequency (3~7 Hz) and gamma-frequency (30~80 Hz) components increased when the states

shifted to higher stages. Figure 7C summarizes the FFT power of the theta- and gamma-frequency ranges (n=17 slices).

Input conductance in different internal states

Previous studies showed that UP depolarization is accompanied by an increase in input conductance, which is generated by synaptic barrages through an active network (Pare et al., 1998; Destexhe et al., 2003; Shu et al., 2003a). We therefore tried to examine whether input conductance and reversal potential vary between different states. We carried out paired recordings in which one neuron was current-clamped to monitor membrane fluctuations, and the other neuron was voltage-clamped at between -60 and 0 mV to measure both input conductance and reversal potential. States IV and V were analyzed because only these two states showed SDSs long enough to measure the membrane conductance precisely.

Representative results are shown in Figure 8A. As UP depolarization started, the input conductance rapidly increased and gradually decreased to a steady state. The reversal potential during SDSs was -40 ~ -20 mV. We calculated the input conductance and the reversal potential by referring the slope and intercept of the I-V plot, respectively. We compared the conductance during the DOWN baseline periods and the UP periods (SDSs) and found that the conductance was increased during UP. This conduction increase (Δconductance) represents an increase in membrane conductance due to synchronized synaptic inputs from active networks, and thus, the Δconductance reflects the level of network activity (Shu et al., 2003a). The change in the reversal potential during UP state, if any, is also due to synaptic inputs, but it reflects the ratio of excitatory and inhibitory inputs, rather than the intensity of synaptic activity (Shu et al., 2003a). Figure 8B summarized the Δconductance and the reversal potential of six cells. The Δconductance in state V was 16.8 ± 5.5 nS (n=6). This value is consistent with Δconductance measured in other studies in cortical UP state *in vitro* (10~15 nS) (Shu et al., 2003a, Fig 2) and *in vivo* (~14 nS) (Pare et al., 1998; we obtained this value based on R_{in} of the UP (the 70% point) and DOWN peaks in Fig. 5 of

their paper). This value was significantly higher than that during UP periods in state IV (6.8 ± 2.0 nS). On the other hand, the reversal potential in state V (-28.0 ± 11.6 mV) was not different from that in state IV (-33.1 ± 8.6 mV). These results suggest that higher neuronal states are associated with higher input conductance whereas the balance of excitatory and inhibitory inputs, captured by reversal potential, is preserved across states.

Modeling the internal states and state transitions of a neuron

We have shown above that 1) the internal state of a CA3 pyramidal cell can shift to a different state in response to stimulation, 2) the cell has higher synaptic input conductance in higher states, and 3) the internal states of nearby neurons are synchronized among the network. These results suggest that the internal state of a single cell reflect the level of synchronous firing activity of the network. For instance, if neuron populations display synchronous firing activity, each neuron in the network receives a higher level of balanced excitatory and inhibitory synaptic inputs, which may contribute to organized fluctuations of membrane potential. On the other hand, neurons receive stochastic synaptic inputs if the network neurons fire randomly. We therefore hypothesize that the internal states of individual neurons reflect the degree of synchrony of the network, i.e., the "phase" of network activity. If this is the case, the transition dynamics of the internal state must be described by a so-called "phase transition" model in solid-state physics. We therefore attempted to create a theoretical model to describe the phase transition dynamics of network synchronization, according to the Landau "phase transition" theory (Landau 1980) and Amit, Gutfreund and Sompolinsky's phase transition model (Amit et al., 1985). Our model describes 1) the structure of synchronous network activity, 2) the internal states of individual cells in the network, and 3) the dynamics produced by their interactions. In this model, we make two assumptions (Fig 9A; see also the supplemental materials);

1) The free-energy of network activity F follows:

$$F = \mu(T - T_c)\varphi^2 + u\varphi^4$$

This formula is based on a phase transition model of the Hopfield network (Hopfield 1982,1984, Amit et al., 1985; Hertz et al., 1991; Nishimori 2001; see also the supplemental materials) although unlike our model, the correlation was given by emission rates, not spiking dynamics, in these previous models (Amit, 1989). φ shows the synchrony level of the network. $\varphi = 0$ means that the network firing activity is random, $\varphi>0$ indicates that the "firing" states of individual neurons are more synchronized, and $\varphi<0$ indicates that more neurons are synchronized at "non-firing" states. μ and u are constants.

T represents a conceptual "pseudo-temperature" of network activity. Note that T is not real temperature, but rather it is used here as a numerical statistic associated with network activity (Hertz et al., 1991); that is, as T is higher, neurons become to act more randomly. In other words, the shape of the free-energy function F changes as a function of T. In this respect, we consider the critical temperature T_c, at which point the number of the stable points (local minima) of the free energy function changes. When network temperature is higher than this critical value (i.e., $T > T_c$), there is one stable point at $\varphi = 0$, whereas there are two stable points when T is less than T_c. This change in the number of stable points represents a "phase transition" of the network synchrony state, i.e., a shift from random states to synchronous firing states (Amit et al., 1985).

2) When the network displays synchronous activity, it generates balanced excitatory and inhibitory synaptic inputs to individual neurons embedded in the network, which cause an increase of membrane conductance of these cells. This assumption comes from our observation (Fig. 8). The details are stated in the supplemental materials.

Fig. 9B shows the results of the computational simulation of this model. When the temperature is higher than the critical temperature ($T > T_c$), the distribution of membrane potential showed a single peak (Fig. 9B). On the other hand, when the temperature is lower than the critical temperature ($T < T_c$), the membrane potential showed a biphasic distribution, and the histogram of SDS durations revealed a $1/s^{\nu}$ structure with an exponent $\nu = 1.09$ (Fig. 9B). These

results are in close agreement with our experimental data. The maximal length of SDSs for any given 10-sec epoch was increased as *T* was decreased, and the relationship was nonlinear (Fig. 9C left). The membrane conductance also became higher as *T* was decreased (Fig. 9C middle). Therefore, SDSs durations were positively correlated with the Δconductance (Fig. 9C right), as we predicted in our working hypothesis. Therefore, our model indicates that the internal state of a neuron indeed represents the phase of network activity and that a transition of the phase depends on the level of balanced input conductance, i.e., the degree of the overall network activity.

DISCUSSION

About 300,000 pyramidal cells exist in the rat CA3 pyramidal cell layer *in vivo* at a density of about 70,000 cells/mm^3 (Amaral et al., 1990; Coburn-Litvak et al., 2004). On average, each pyramidal cell projects to about 6,000 other pyramidal cells, a significant portion of which are located within a few millimeter radius. Thus, the probability that cell pairs located within 500 μm are synaptically connected is calculated to be roughly 10-25% (Gomez-Di Cesare et al., 1997). Consistent with this, we found that out of 42 recordings from pairs of cells located within 300 μm, 23.8% (10/42) showed monosynaptic connection. In acute slice preparations, this probability is quite low (data not shown) because the slicing procedure cuts CA3 associational fibers extending in the longitudinal axis of the hippocampus. Axonal reorganization in organotypic cultures restores the complexity of CA3 recurrent loops to a realistic extent, so we believe that our data reflect the physiological operations of CA3 recurrent networks.

Using this preparation, we have shown that CA3 neurons involve multiple internal states defined by the dynamics of subthreshold membrane potential. Different internal states show different spiking behaviors and different sensitivity to external inputs; in particular, neurons with state IV exhibit typical UP/DOWN alternations, and their membrane dynamics are characterized by various power-law features and a U-shaped ISI distribution. Following evoked spiking in

single cells, network neurons move between internal states. Thus, the state of any given neuron may report on and influence the state of the local network.

We found that the generation of synchronous network activity is related to self-organization typified by a 1/s power law. The power-law distribution, also called scale-free, is present in many natural systems; it is thought to reflect the cluster growth pattern with self-similar features in time and space and usually emerges as a critical phenomenon in the complex system (Bak et al., 1987). The power law structure has recently been observed in propagating waves of synchronous firing in neocortical slices (Beggs and Plenz, 2003). We found that power laws are also evident in intracellular responses, i.e., SDS durations and ISIs (Fig. 3B), implying that membrane fluctuations of neurons are self-organized.

Internal states *in vivo* and *in vitro*

Coherent fluctuations of membrane potential have been associated with brain states. In the neocortex, slow-wave oscillations, i.e., UP/DOWN alternations, appear in slow-wave sleep, and persistent UP depolarization in REM sleep and awake conditions (Steriade 2003). In the hippocampus, theta oscillations occur in REM sleep and waking exploration but are absent in slow-wave sleep and resting conditions (Buzsaki 2002). These facts suggest that information processing is state- and region-dependent (Stickgold et al., 2001).

We categorized the internal states of neurons into five classes. Based on their dynamics, we consider that states I and II correspond to persistent DOWN (or basal) states, state III may be related to complex burst spikes often seen in CA3 pyramidal cells in behaving animals, state IV is UP/DOWN alternations, and state V is persistent UP depolarization. Specifically, in the hippocampus, theta and non-theta states seem to be the only states seen *in vivo* (Isomura et al., 2004). The theta state may correspond to state V, and the non-theta to state I-III because theta oscillations were more prominent in state V. In this sense, state IV is unique and could represent a transition stage between them. Indeed, our findings are the first evidence that hippocampal

neurons are potentially capable of rapidly alternating between UP and DOWN, like neurons in the neocortex, thalamus, and striatum.

Network-dependent changes in membrane conductance

A fundamental issue is how membrane potential fluctuations, such as UP/DOWN alternations, are generated in a single cell, and how these fluctuations are synchronized within the network. Macroscopic membrane conductance, which consists of synaptic channels such as AMPA, NMDA, and $GABA_A$ receptors (Shu et al., 2003a) and non-synaptic channels such as persistent Na^+ and I_H channels (Mao et al., 2001; Compte et al., 2003; Loewenstein et al., 2005), appears to be critical in generating the complex SDS dynamics. Shu et al. (2003a) and we carefully measured the reversal potential during UP depolarization and demonstrated that the elevated conductance is comprised of proportionally balanced synaptic excitation and inhibition and sustained through local recurrent synaptic connections. Consistent with this, membrane potential fluctuation of a pyramidal cell was abolished by a cocktail of antagonists of synaptic receptors. Therefore, SDSs are generated predominantly by an increase in synaptic conductance, i.e., synaptic bombardment. Since the input conductance in state V was larger than that in state IV, but the reversal potential was unchanged; as the internal states advance to higher levels, synaptic bombardments during UP depolarization becomes more intensive without changing the total balance of excitatory and inhibitory inputs. In other words, the duration of SDSs reflects the total amount of balanced network activity.

Because GABAergic interneurons are present in our preparations and also because they seem to play a pivotal role in network synchronization (Traub et al., 2004), it is possible that the local inhibition determined the level of balanced network activity. Further studies are required to address this possibility, but it is consistent that intracellular recordings in ferret prefrontal cortical neurons during UP periods revealed that strong barrages of IPSPs were often synchronized between neighboring pyramidal cells and that the dynamic-clamp intracellular injection of

simulated IPSP barrages strongly influenced spike timing (Hasenstaub et al., 2004).

The fact that the durations of SDSs vary as a function of input conductance implies that a change in weights of individual synapses, i.e., synaptic plasticity, is not necessary for state transitions, that is, it is the level of synaptic bombardment (i.e., how many synapses are simultaneously active), rather than individual synaptic strength or efficacy, that determines the state of a neuron. This may explain why activation of single neurons alone can alter the state of the entire local network; note that synaptic plasticity is usually an extremely localized phenomenon with input specificity and would therefore be unable to explain the results of single cell-induced entrainment of network activity. We speculate that the input conductance generated by network activity itself is plastic, thereby achieving self-sustained multistability of the internal states. Given that the responsiveness to external stimuli depends on internal states, it is balanced input conductance that regulates network performance in information processing.

Our finding that neuronal states and their transition dynamics occur as a result of active recurrent network operations provides a novel type of circuit plasticity, i.e., persistent changes in network excitability, which differs from plasticity supported by the intrinsic properties of single cells, such as “graded persistent activity” in the neocortex (Egorov et al., 2002) or “windup” in the spinal cord (Morisset and Nagy, 2000). Activation of single neurons has been reported to transiently recruit the correlated activity of a network (Miles and Wong 1983; Brecht et al., 2004; Briggman et al., 2005), but our results indicate that single neurons are also capable of modifying ongoing network activity, an effect that persists for long periods and could affect network responsiveness.

From attractors to phases

As discussed above, the internal state of a neuron, defined by SDSs, represents the state of the local network, i.e., “macroscopic attractors”. On the other hand, information processing such as memory storage and association has so far been believed to depend on “microscopic attractors”,

in which individual neurons act as attractors in the network. Such microscopic attractors were experimentally proposed by Mainen and Sejnowski (1995), but it remains largely unknown how they indeed contribute to information processing. Hopfield has theoretically indicated that microscopic attractors embody associative memory in a neural network (Hopfield, 1982, 1984). In his model, synaptic weights between neurons in an associative network determine the stability and patterns of synchronous firing of a subset of neurons, i.e., cell assembly. In other words, the connectivity of a network produces a stable synchrony of neuron ensembles. This is in essence equivalent to the Ising model in statistical solid-state physics. Spikes or no spikes in the Hopfield model correspond to spin orientation ("up" or "down") of electrons in the Ising model, and the connectivity of a network in the Hopfield model corresponds to the interaction between spins (Hertz et al., 1991). In the Ising model, phase transitions of magnetic are explained by a change in the statistical nature of spin interaction, which is induced by a temperature change (Onsager 1944). Likewise, in Hopfield model, a change in the level of network activity, termed "pseudo-temperature *T*", induces a phase transition of synchrony patterns in the Hopfield network (Amit et al., 1985).

In our model, we made the working hypothesis that the internal state of a neuron reflects the "phase" of synchronous network activity, that is, membrane potential fluctuations of single cells are determined by synaptic input conductance that is produced by synchronous network activity. By using mean-field approximation of the Hopfield model, we succeeded in describing attractor dynamics of synchronous network activity in the macroscopic level. From a statistical physics point of view, we have depicted, for the first time, the behavior of a neural network in a way that is consistent with experimental data. Note that the Hopfield model has not yet been physiologically verified in the biological system, and therefore, this is the first proven case in which a phase transition model is linked to experimental data.

Conclusions

We have experimentally revealed details of internal neuronal states and their dynamics. These states include persistent activity, UP/DOWN alternations, and theta and gamma oscillations. We see these different phenomena as reflections of synchronous activity in a recurrent network with the internal states developing through the nonlinear dynamics of a complex system with self-organized criticality. These behaviors of a neuron can elegantly be expressed in the physical formula of phase transitions, and hence, we propose herein that the internal state of a neuron is regarded as a reflection of the "phase" of a biological neural network.

REFERENCES

Amaral DG, Ishizuka N, Claiborne B (1990) Neurons, numbers and the hippocampal network. Prog Brain Res 83: 1-11.

Amit DJ (1989) Modeling Brain Function, Cambridge University Press, Cambridge England and New York

Amit DJ, Gutfreund H, Sompolinsky H (1985) Storing infinite numbers of patterns in a spin-glass model of neural networks. Physl Rev Lett 55: 1530-1533.

Amit DJ, Brunel N (1997) Model of global spontaneous activity and local structured activity during delay periods in the cerebral cortex. Cereb Cortex 7: 237-52.

Anderson J, Lampl I, Reichova I, Carandini M, Ferster D (2000) Stimulus dependence of two-state fluctuations of membrane potential in cat visual cortex. Nat Neurosci 3: 617-621.

Bak P, Tang C, Wiesenfeld K (1987) Self-Organized Criticality - An Explanation of 1/F Noise. Physl Rev Lett 59: 381-384.

Beggs JM, Plenz D (2003) Neuronal avalanches in neocortical circuits. J Neurosci 23: 11167-11177.

Brecht M, Schneider M, Sakmann B, Margrie TW (2004) Whisker movements evoked by stimulation of single pyramidal cells in rat motor cortex. Nature 427: 704-710.

Briggman KL, Abarbanel HD, Kristan WB, Jr. (2005) Optical imaging of neuronal populations during decision-making. Science 307: 896-901.

Buzsaki G (2002) Theta oscillations in the hippocampus. Neuron 33: 325-340.

Coburn-Litvak PS, Tata DA, Gorby HE, McCloskey DP, Richardson G, Anderson BJ (2004) Chronic corticosterone affects brain weight, and mitochondrial, but not glial volume fraction in hippocampal area CA3. Neuroscience 124: 429-438.

Compte A, Sanchez-Vives MV, McCormick DA, Wang XJ (2003) Cellular and network mechanisms of slow oscillatory activity (<1 Hz) and wave propagations in a cortical network model. J Neurophysiol 89: 2707-2725.

Cowan RL, Wilson CJ (1994) Spontaneous firing patterns and axonal projections of single corticostriatal neurons in the rat medial agranular cortex. J Neurophysiol 71: 17-32.

Crochet S, Chauvette S, Boucetta S, Timofeev I (2005) Modulation of synaptic transmission in neocortex by network activities. Eur J Neurosci 21: 1030-1044.

Destexhe A, Rudolph M, Pare D (2003) The high-conductance state of neocortical neurons in vivo. Nat Rev Neurosci 4: 739-751.

Egorov AV, Hamam BN, Fransen E, Hasselmo ME, Alonso AA (2002) Graded persistent activity in entorhinal cortex neurons. Nature 420: 173-178.

Fisahn A, Pike FG, Buhl EH, Paulsen O (1998) Cholinergic induction of network oscillations at 40 Hz in the hippocampus in vitro. Nature 394: 186-189.

Fujisawa S, Matsuki N, Ikegaya Y (2004) Chronometric readout from a memory trace: gamma-frequency field stimulation recruits timed recurrent activity in the rat CA3 network. J Physiol 561: 123-131.

Fujisawa S, Yamada MK, Nishiyama N, Matsuki N, Ikegaya Y (2004) BDNF boosts spike fidelity in chaotic neural oscillations. Biophys J 86: 1820-1828.

Gomez-Di Cesare CM, Smith KL, Rice FL, Swann JW (1997) Axonal remodeling during postnatal maturation of CA3 hippocampal pyramidal neurons. J Comp Neurol 384: 165-180.

Hasenstaub AR; Haider B Duque A, McCormick DA (2004) Control of neuronal sensory responsiveness and spike timing by local recurrent activity. Program No. 985.15. 2004 Abstract Viewer and Itinerary Planner. Washington, DC: Society for Neuroscience, Online.

Harris KD, Hirase H, Leinekugel X, Henze DA, Buzsaki G (2001) Temporal interaction between single spikes and complex spike bursts in hippocampal pyramidal cells. Neuron 32: 141-149.

Hertz J, Krogh A, Palmer RG (1991) Introduction to the theory of neural computation. New York: Westview Press.

Hopfield JJ (1982) Neural networks and physical systems with emergent collective computational abilities. Proc Natl Acad Sci U S A 79: 2554-2558.

Hopfield JJ (1984) Neurons with graded response have collective computational properties like those of two-state neurons. Proc Natl Acad Sci U S A 81: 3088-3092.

Ikegaya Y, Aaron G, Cossart R, Aronov D, Lampl I, Ferster D, Yuste R (2004) Synfire chains and cortical songs: temporal modules of cortical activity. Science 304: 559-564.

IsomuraY, Hirase H, Sirota AM, Buhl DL, Buzsaki G. (2004) Subicular, anterior cingulate, and prefrontal activity associated with hippocampal ripples and theta oscillations. Program No. 550.4. 2004 Abstract Viewer and Itinerary Planner. Washington, DC: Society for Neuroscience, Online.

Kamondi A, Acsady L, Wang XJ, Buzsaki G (1998) Theta oscillations in somata and dendrites of hippocampal pyramidal cells in vivo: Activity-dependent phase-precession of action potentials. Hippocampus 8: 244-261.

Koyama R, Yamada MK, Fujisawa S, Katoh-Semba R, Matsuki N, Ikegaya Y (2004) Brain-derived neurotrophic factor induces hyperexcitable reentrant circuits in the dentate gyrus. J Neurosci 24: 7215-7224.

Lampl I, Reichova I, Ferster D (1999) Synchronous membrane potential fluctuations in neurons of the cat visual cortex. Neuron 22: 361-374.

Landau LD, Lifshitz EM, Pitaevskii LP (1980) Statistical physics. New York: Pergamon.

Leger JF, Stern EA, Aertsen A, Heck D (2005) Synaptic integration in rat frontal cortex shaped by network activity. J Neurophysiol 93: 281-293.

Loewenstein Y, Mahon S, Chadderton P, Kitamura K, Sompolinsky H, Yarom Y, Hausser M (2005) Bistability of cerebellar Purkinje cells modulated by sensory stimulation. Nat Neurosci 8: 202-211.

Mainen ZF, Sejnowski TJ (1995) Reliability of Spike Timing in Neocortical Neurons. Science 268: 1503-1506.

Mao BQ, Hamzei-Sichani F, Aronov D, Froemke RC, Yuste R (2001) Dynamics of spontaneous activity in neocortical slices. Neuron 32: 883-898.

Miles R, Wong RK (1983) Single neurones can initiate synchronized population discharge in the hippocampus. Nature 306: 371-373.

Morisset V, Nagy F (2000) Plateau potential-dependent windup of the response to primary afferent stimuli in rat dorsal horn neurons. Eur J Neurosci 12: 3087-3095.

Nishimori H (2001) Statistical Physics of Spin Glasses and Information Processing: An Introduction. New York: Oxford University Press.

Onsager L (1944) Crystal Statistics. I. A Two-Dimensional Model with an Order-Disorder Transition. Phys Rev 65: 117-149.

Ott E (1993) Chaos in Dynamical Systems. New York: Cambridge University Press.

Pare D, Shink E, Gaudreau H, Destexhe A, Lang EJ (1998) Impact of spontaneous synaptic activity on the resting properties of cat neocortical pyramidal neurons In vivo. J Neurophysiol 79: 1450-1460.

Petersen CC, Hahn TT, Mehta M, Grinvald A, Sakmann B (2003) Interaction of sensory responses with spontaneous depolarization in layer 2/3 barrel cortex. Proc Natl Acad Sci U S A 100: 13638-13643.

Sachdev RNS, Ebner FF, Wilson CJ (2004) Effect of subthreshold up and down states on the whisker-evoked response in somatosensory cortex. J Neurophysiol 92: 3511-3521.

Shu Y, Hasenstaub A, Badoual M, Bal T, McCormick DA (2003) Barrages of synaptic activity control the gain and sensitivity of cortical neurons. J Neurosci 23: 10388-10401.

Shu YS, Hasenstaub A, McCormick DA (2003) Turning on and off recurrent balanced cortical activity. Nature 423: 288-293.

Steriade M, Timofeev I, Grenier F (2001) Natural waking and sleep states: a view from inside neocortical neurons. J Neurophysiol 85: 1969-1985.

Steriade M (2003) Neuronal substrates of sleep and epilepsy. Cambridge: Cambridge Univ Press.

Steriade M, Nunez A, Amzica F (1993) A Novel Slow (Less-Than-1 Hz) Oscillation of Neocortical Neurons In-Vivo - Depolarizing and Hyperpolarizing Components. J Neuroscie 13: 3252-3265.

Stern EA, Jaeger D, Wilson CJ (1998) Membrane potential synchrony of simultaneously recorded striatal spiny neurons in vivo. Nature 394: 475-478.

Stickgold R, Hobson JA, Fosse R, Fosse M (2001) Sleep, learning, and dreams: off-line memory reprocessing. Science 294: 1052-1057.

Traub RD, Bibbig A, Lebeau FEN, Buhl EH, Whittington MA (2004) Cellular mechanisms of neuronal population oscillations in the hippocampus in vitro. Ann Rev of Neurosci 27: 247-278.

Vaadia E, Haalman I, Abeles M, Bergman H, Prut Y, Slovin H, Aertsen A (1995) Dynamics of Neuronal Interactions in Monkey Cortex in Relation to Behavioral Events. Nature 373: 515-518.

Wilson MA, Mcnaughton BL (1994) Reactivation of Hippocampal Ensemble Memories During Sleep. Science 265: 676-679.

FIGURE LEGENDS

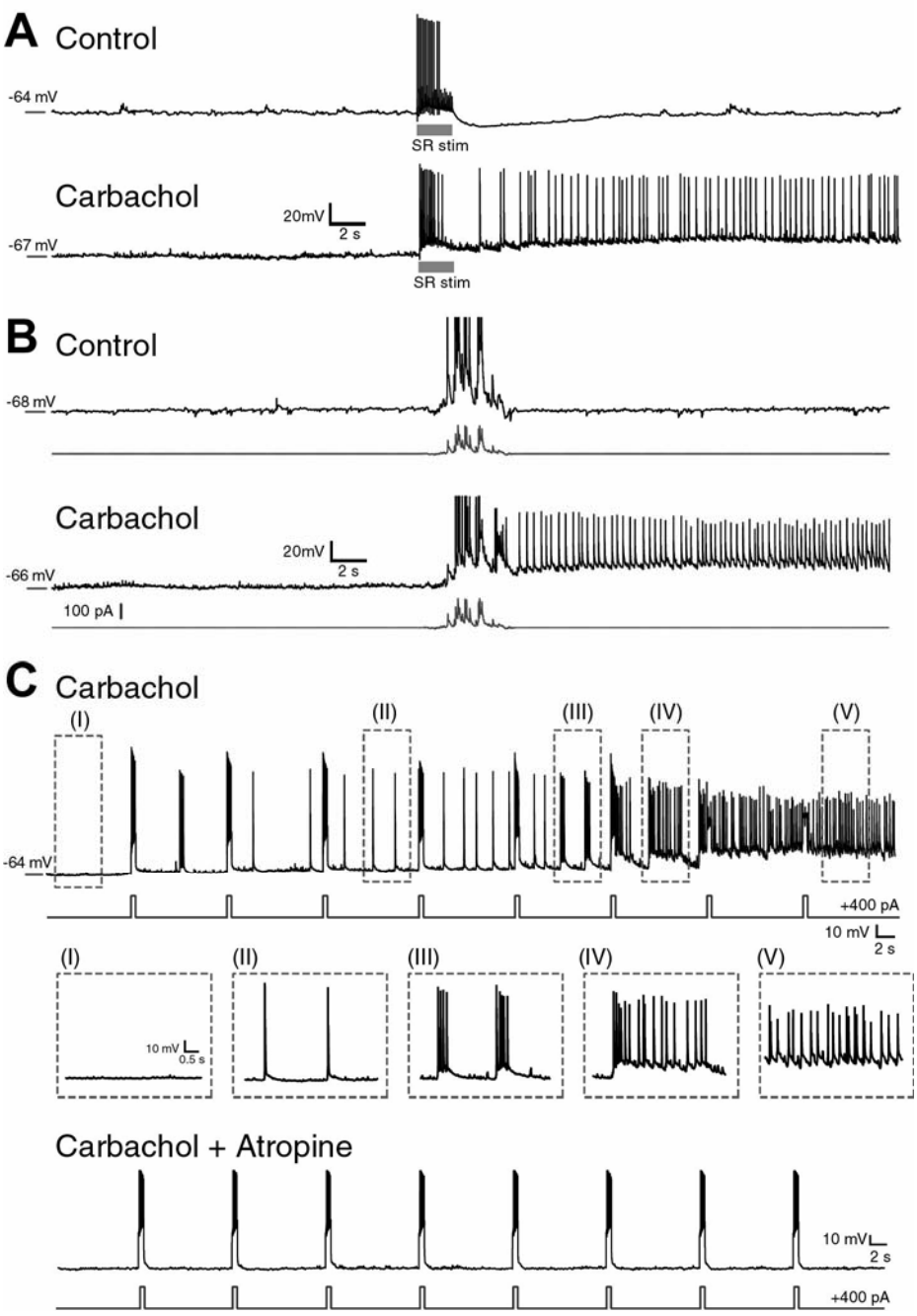

Figure 1 CA3 pyramidal cells transit between multiple active states **A.** A current clamp trace from a CA3 pyramidal neuron in the absence (*top*) and presence of 10 μM carbachol (*bottom*). A persistent depolarizing shift with continuous firing activity was induced by a 10-Hz, 2-sec stimulus of the stratum radiatum (SR stim.) only in the presence of carbachol. **B.** A similar depolarizing shift was induced by current injection into a neuron, in the presence of, but not in the absence of (*top*), 10 μM carbachol (*bottom*). The current profile mimicked the temporal structure of a post-synaptic potential barrage. **C.** Repetitive injections of brief rectangular currents (500 ms, 400 pA, every 10 sec) in the presence of 10 μM carbachol induced a gradual change in firing patterns, eventually leading to self-sustained tonic discharges. Middle: magnified views of portions of the recording indicated by correspondingly numbered boxes above. Bottom: this gradual change in firing patterns did not occur in the presence of the muscarinic receptor agonist atropine (atropine 1 μM, carbachol 10 μM).

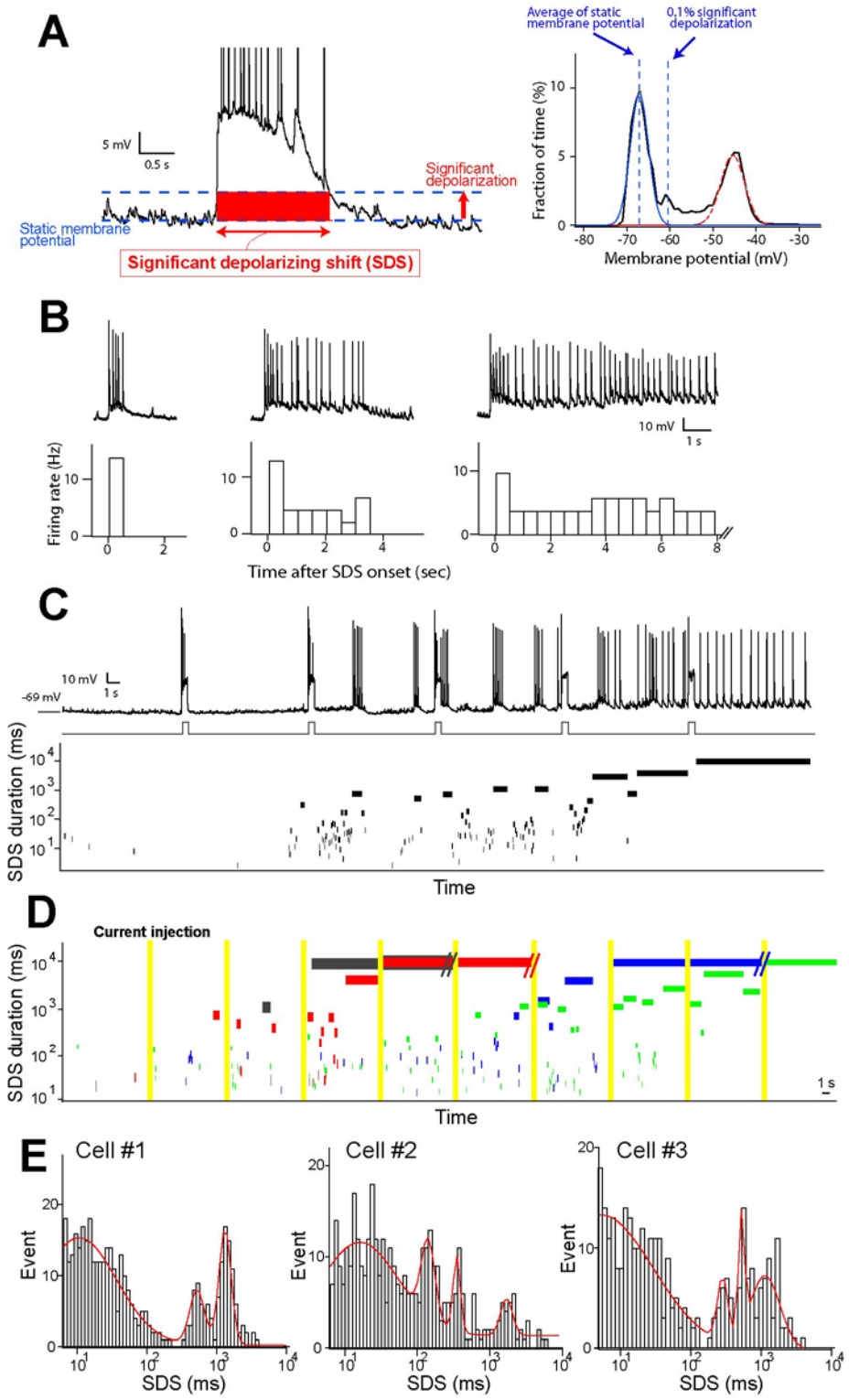

Figure 2 Internal states of neurons are defined by significant depolarizing shifts (SDSs) **A.** Definition of the significant depolarizing shift (SDS). The frequency of membrane potential was bimodal, fitted by two Gaussian curves (right); the first peak (blue) represents the resting membrane potential, and the second peak (red) corresponds to UP depolarization. Here we define the "significant depolarizing shift (SDS)" as membrane potential above the 0.1% significance level of the Gaussian fitting the non-depolarized (resting) membrane potential. Henceforth, SDSs will be classified based on their durations. **B.** Relationship between firing rate and SDS durations. **C.** Membrane potential dynamics (top) of a neuron that received repetitive current injections (500 ms, 400 pA, every 10 sec) was analyzed by plotting the SDS durations versus time (bottom). **D.**

Current injection-evoked changes in SDSs of four cells obtained from different slices. Each color represents each neuron. **E.** The distribution of SDS duration of CA3 pyramidal showed multiple peaks. Data were obtained from different slices. These data suggest that internal states of cells are not completely continuum, but have some dispersal and distinct features. Experiments were performed in the presence of 10 μM carbachol.

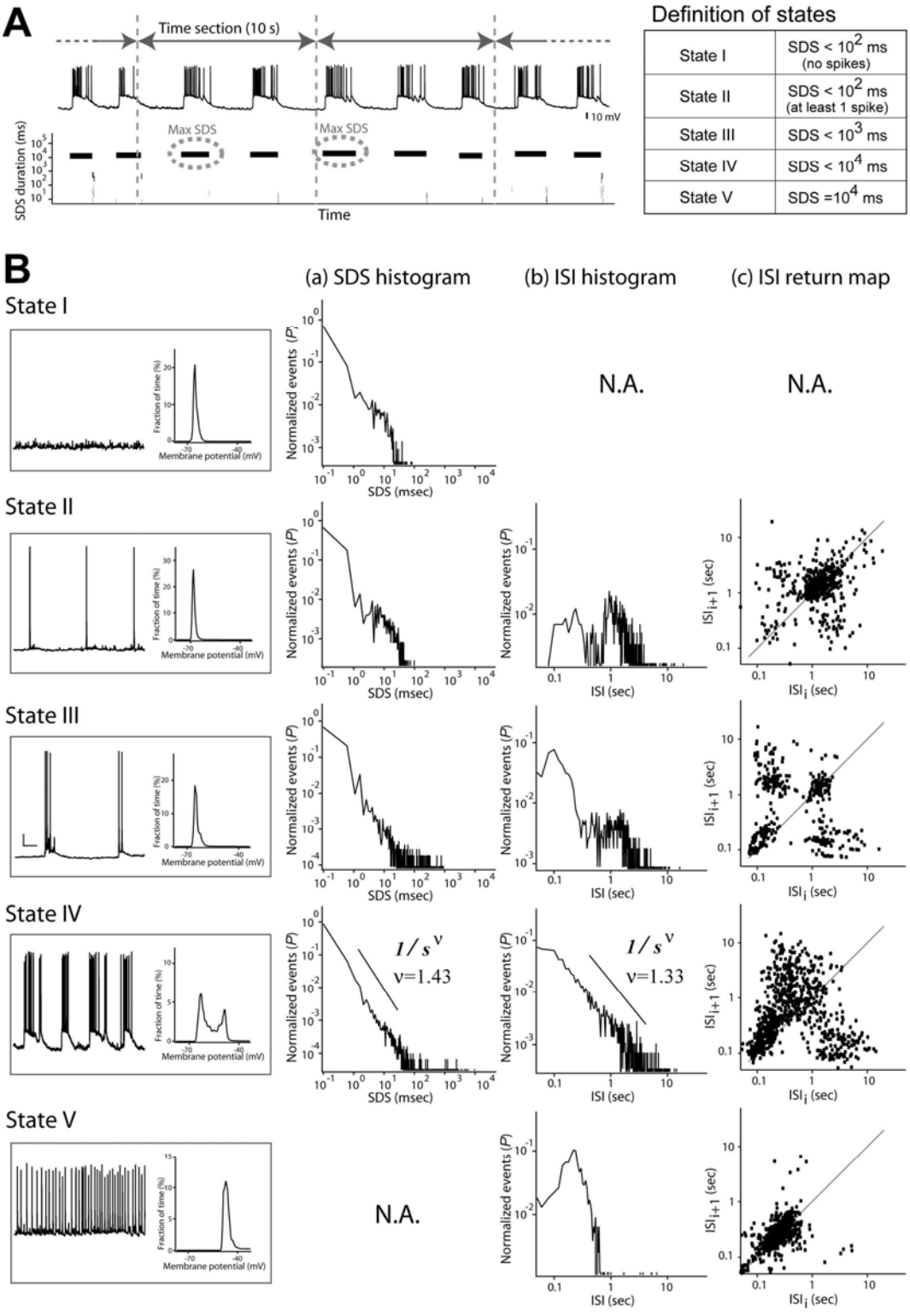

Figure 3 Internal states are diverse and often self-organized. A. Network states are categorized based on the maximal length of SDS involved in a 10-sec segment of an intracellular trace. State I is defined as any 10-sec period during which the maximal SDS is less than 100 msec and no spike occurs. State II is defined as any 10-sec period during which the maximal SDS is less than 100 msec and at least one spike occurs. States III and IV are defined as any 10-sec period during which the maximal SDS is between 100 msec and 1 sec or between 1 sec, and 10 sec, respectively. State V is defined when the SDS persists for the entire 10-sec period. **B.** Characterization of the internal states. Left panels show representative waveforms and their membrane potential histograms. Scale bar: 10 mV, 2 sec. (a) The middle-left panels indicate the frequency of the SDS duration for each state. State IV shows a $1/s^{\nu}$ structure with ν=1.43. (b) The middle right histograms indicate the frequency of inter-spike intervals (ISIs). State IV shows a $1/f^{\nu}$ structure with ν=1.33. (c) The right panels indicate first-return maps of ISIs, in which ISIs are plotted against the next ISIs. State IV shows a typical bell-shaped distribution, indicative of deterministic chaos. N.A.: not analyzed. Experiments were performed in the presence of 10 μM carbachol.

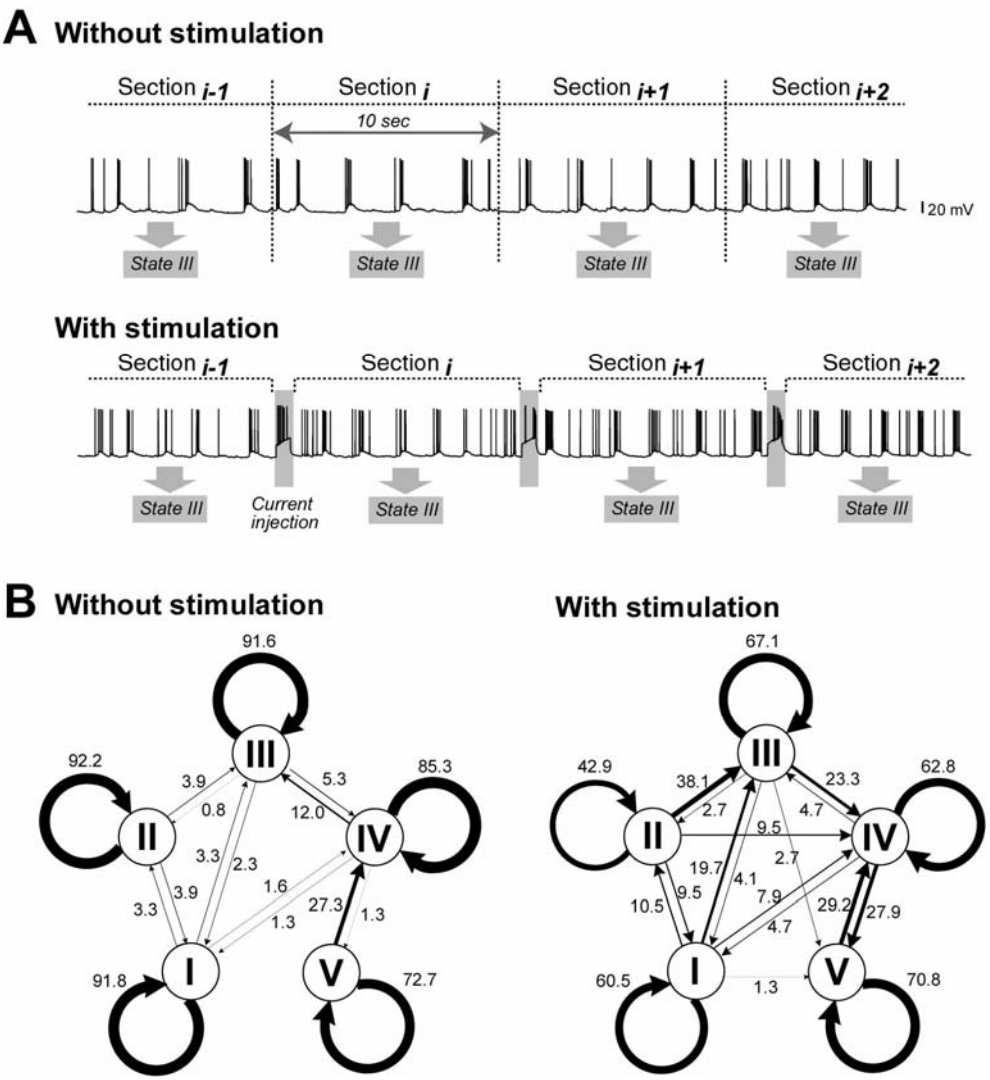

Figure 4 Transition probability of internal states A. Schematics for calculation of the transition rate. In the case of 'without stimulation', we arbitrarily segmented an intracellular trace into consecutive time epochs of 10 sec and classify each epoch into one of five states as defined in Fig. 3A, and then we calculate the rate of state transitions between neighboring 10-sec epochs (*top*). In the case of 'with stimulation', we performed current injection between the sections (*bottom*) **B.** Ratios of state transitions in the absence (without stimulation) and presence of brief current injection (with stimulation). The numbers I, II, III, IV, and V indicate the corresponding states. Spontaneous transitions are compared between consecutive 10-sec epochs in an intracellular recording. Evoked transitions are compared between the 10-sec periods before and after any current injection. The numbers on the arrows indicate the percentages of state transitions from each initial state (N = 34 cells). Without current injections, the states tended to stay at the same state as the previous one whereas current injections more often provoked state transitions. Experiments were performed in the presence of 10 μM carbachol.

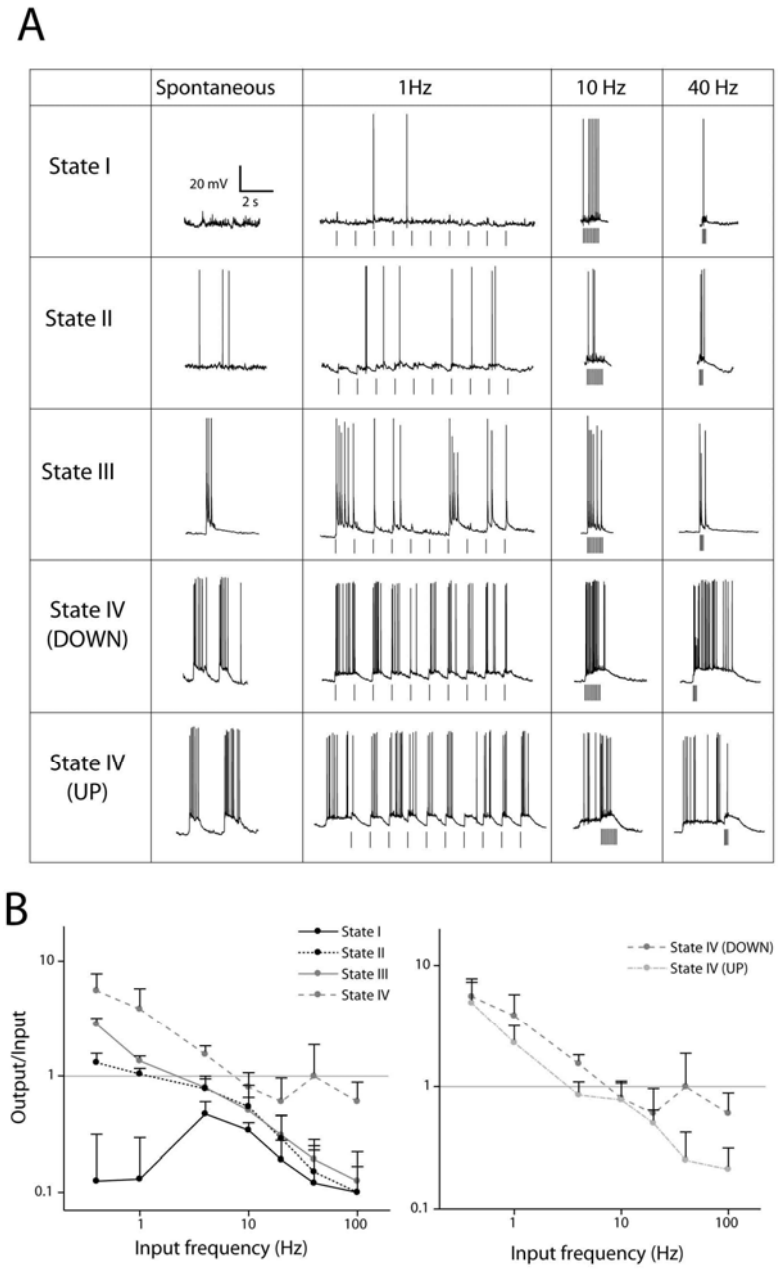

Figure 5 Spiking responses to mossy fiber inputs depend on the input frequency and network states A. Responses to successive 10 stimuli of the mossy fibers at 1, 10, and 40 Hz in each state. **B.** Relationship between the output/input ratio (gain) and stimulation frequency in each state. The output/input ratio was defined as the number of spike emissions per stimulus. As neurons transit to higher states, they became responsive to lower-frequency mossy fiber inputs (≤ 1 Hz). During DOWN periods in state IV, neurons respond sensitively to high-frequency inputs (≥ 40 Hz). N=7 slices. Experiments were performed in the presence of 10 μM carbachol.

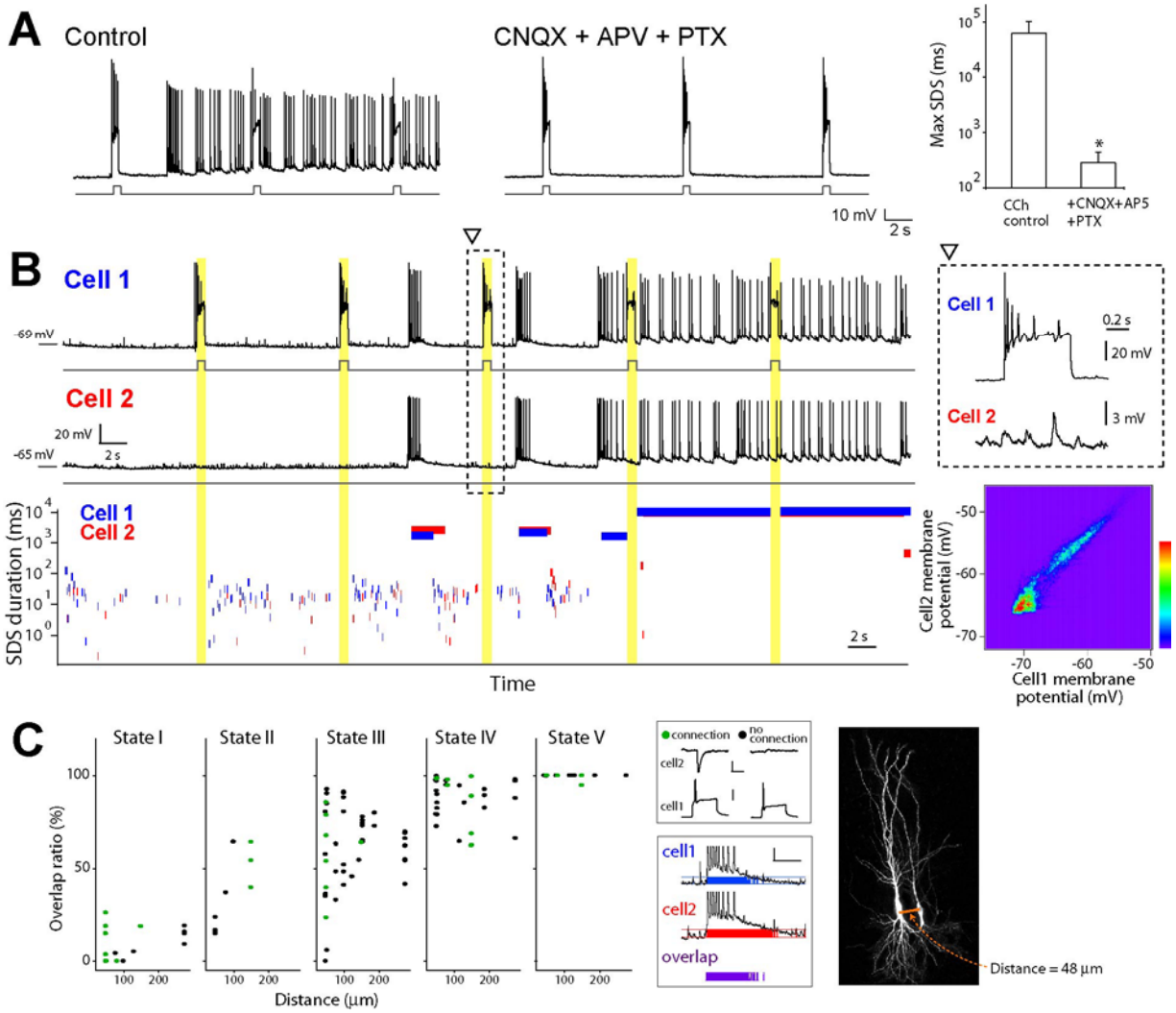

Figure 6 State transitions are network-driven and can be triggered by activation of single cells A. Intracellular traces of CA3 pyramidal cells that received repetitive current injections in the presence of 20 µM CNQX, 50 µM D,L-AP5 and 100 µM PTX (*Left*). The right panel indicates the maximal SDS durations seen during a sequence of current injections (7 times, 10 second intervals) in the absence and presence of the inhibitor cocktail. No state transition occurs in the presence of the inhibitor cocktail, indicating that the states are not attributable to single-cell attractors. *$P < 0.05$ versus control, Student's *t*-test ($N = 5$ cells). **B.** Membrane potential waveforms recorded simultaneously from a pair of neighboring CA3 pyramidal cells (*top left*). A part of the trace is expanded (open triangle), showing no monosynaptic connection from cell1 to cell2 (*top right*). Current injections into cell1 alone induced concurrent transitions of the states in both cells. The bottom-left plot indicates SDS durations of these two cells as a function of time. The bottom-right panel indicates a two-dimensional pseudo-color plot of subthreshold membrane potentials of these cells. **C.** The relationship between the coincidence of SDSs and the distance of two cells recorded. The ordinate indicates the fraction (%) of time that two cells simultaneously spent in SDSs. The green and black dots indicate synaptically connected and unconnected cell pairs, respectively. *Inserts: (Left top)* The existence of direct synaptic connections from cell 1 to cell 2 is confirmed with monosynaptic responses of cell2 following action potential of cell1. Scale bar: 20 pA, 40 mV, 50 msec. (*Left bottom*) Schematics of SDS overlap between cell 1 and cell 2. Scale bar, 5 mV, 1sec. (*Right*) Representative confocal image of a pair of CA3 pyramidal cells that were labeled with streptavidin during recording. Experiments were performed in the presence of 10 µM carbachol.

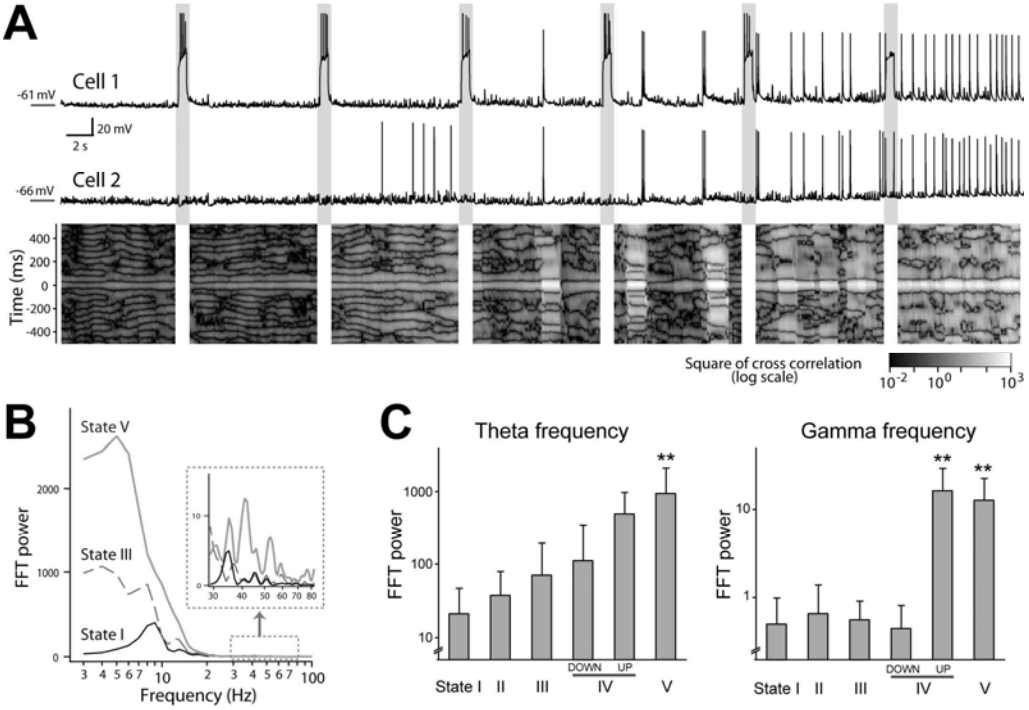

Figure 7 Internal states are associated with theta and gamma oscillations **A.** Membrane potential of cell1 (i.e., the current injected cell) and cell2, and the square of cross-correlogram of the subthreshold membrane potential between cell1 and cell2. **B.** FFT power spectra of the cross-correlogram between cell1 and cell2 in the State I, III, and V (the same neuron as the panel **A**). The power in theta frequency of the cross-correlogram varied as the state changed. **C.** FFT spectrum of cross-correlogram between cell1 and cell2 under the different states. The frequency ranges of theta band (3~7 Hz) and gamma band (30~80 Hz) were analyzed. Experiments were all performed in the presence of 10 μM carbachol.

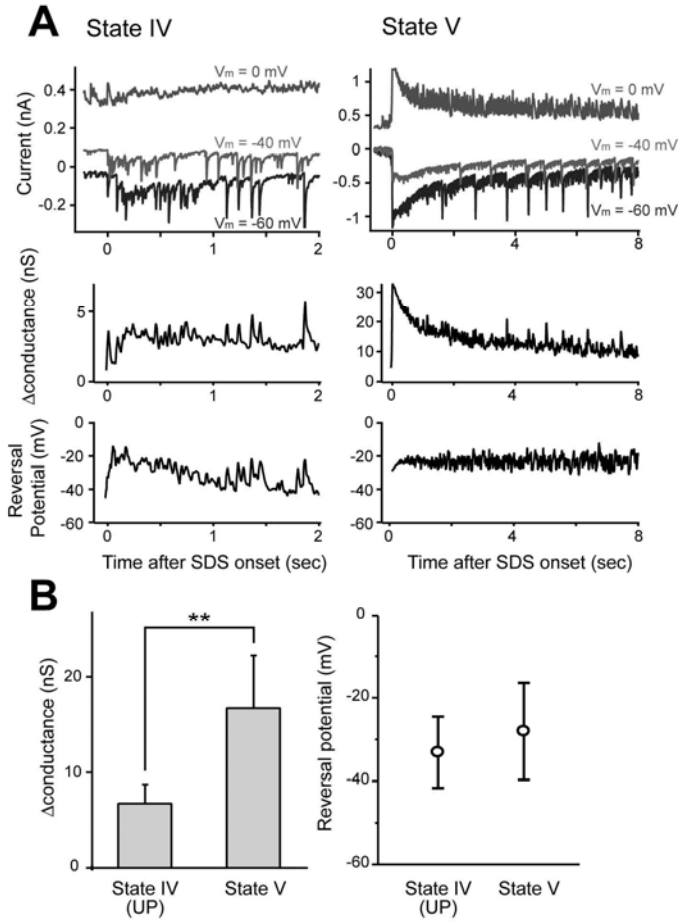

Figure 8 Larger input conductance in neurons during higher level internal states. **A.** Current (*top*), membrane conductance (*middle*) and reversal potential (*bottom*) during spontaneously occurring SDSs in state IV (*left*) and state V (*right*) in the same cells. The internal solution contained 5 mM QX-314 to minimize Na^+ spikes. We measured the membrane conductance based on the slope of the I-V plot and calculated the increase in the conductance during UP periods (Δconductance) by subtracting the conductance in the DOWN baseline from that in UP periods. The baseline conductance during DOWN periods was 9.7 ± 2.8 nS (mean ± SD). Conductance and reversal potential were averaged for 1 sec (UP: from 200 to 1200 ms after the SDS onset. DOWN: from -1200 to -200 ms after the SDS onset). **B**. The Δconductance (*left*) and reversal potential (*right*) in state IV and state V were averaged for a 1-sec period (from 200 to 1200 ms after the onsets of individual SDSs) for each cell. The Δconductance was significantly larger in state V than state IV, but the reversal potential was unchanged. Experiments were performed in the presence of 10 μM carbachol. $^{**}P < 0.01$ versus state IV, paired *t*-test ($N = 6$ cells).

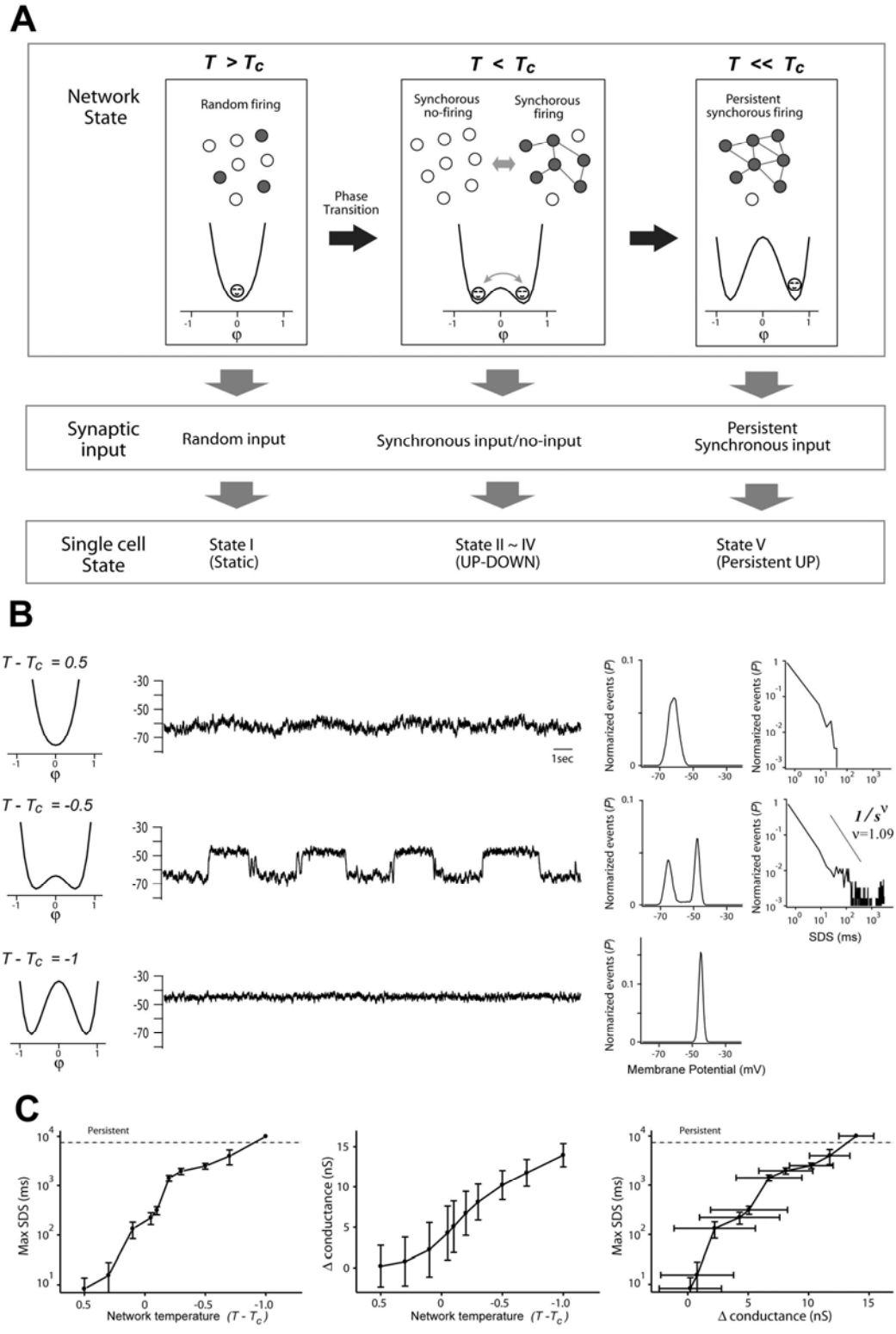

Figure 9 Network states are associated with balanced recurrent activity: a model study inspired by the non-equilibrium statistical theory **A.** Conceptual schematics of our model. This theoretical model describes the relationship between the structure of synchronous network activity and the internal state of single cells in the network. We made the following assumptions: 1) the free-energy of network activity F is given by $F = \mu(T - T_c)\varphi^2 + u\varphi^4$. The network state parameter φ represents the synchronous state of the network, and T the pseudo-temperature of the network activity. T_c is the critical temperature. The shape of the free-energy function changes as a function of T; in particular, the stable point of the free energy function bifurcate at T below the critical temperature T_c, that is, there are two stable points at $T < T_c$. The change in the number of the stable points is called a "phase transition". 2) Synchronous network activity generates balanced excitatory and inhibitory synaptic inputs to each neuron in the network, which cause an increase of membrane conductance of single cells. For details see text and supplemental materials. **B.** Membrane potential fluctuations and histograms of SDS durations are plotted for five T points, i.e., $T > T_c$ (top), $T < T_c$ (top middle, middle, bottom middle), and $T << T_c$ (bottom). The left panels show the shapes of the free energy functions. The middle-left panels indicate typical waveforms of subthreshold membrane potential obtained by computer simulation. The middle-right panels indicate the histograms of membrane potential. The right panels indicate the histograms of SDS durations. For details see text and supplemental materials **C.** Relationship between the network temperature T, Δconductance $g_{balanced}$, and the maximal SDS duration in any 10-sec sections.